Sharif University of Technology

Scientia Iranica

Transactions on Computer Science & Engineering and Electrical Engineering

https://scientiairanica.sharif.edu

A novel mega-stable system with attractors in real-life object shapes

Tayebe Moalemi [a], Atefeh Ahmadi [a], Sajad Jafari [a, b, *], Guanrong Chen [c]

a. Department of Biomedical Engineering, Amirkabir University of Technology (Tehran Polytechnic), Tehran, Iran.
b. Health Technology Research Institute, Amirkabir University of Technology (Tehran Polytechnic), Tehran, Iran.
c. Department of Electrical Engineering, City University of Hong Kong, Hong Kong SAR, China.

* Corresponding author: sajadjafari@aut.ac.ir (S. Jafari)

Received 30 July 2022; Received in revised form 9 January 2023; Accepted 16 April 2023

Keywords

Mega-stability;
Dynamical system;
Attractor;
Attraction basin;
Nonlinear dynamics.

Abstract

This paper introduces a two-dimensional autonomous mega-stable dynamical system with trigonometric nonlinearities. The nonlinearity of this system is induced by tangent hyperbolic and cosine functions. A remarkable feature of this system is the ability to generate very rich patterns of coexisting attractors via the variation of its parameters. Interestingly the shapes of its coexisting attractors resemble some real-life objects, such as Persian rugs, nuts (mainly chestnut), fruits (especially pear), and vegetables (pumpkin and onion). Simulations demonstrate the coexisting attractors, basins of attractions, and real-life object shapes. Moreover, the fixed points of the proposed system, their stability, and the energy dissipation for various pairs of parameters are investigated. Finally, the feasibility of this system is approved by analog circuit simulations. Regarding the high flexibility of this system, producing a broad range of attractor patterns, it could be applied in various fields.

1. Introduction

Dynamical systems produce trajectories of points in space-time with various geometric shapes representing the evolution of complex dynamics in physical, chemical, and biological fields [1]. At any instant, a dynamical system has a state that can be expressed by a set of real numbers as a point in a suitable state space (a geometric manifold) [2]. Corresponding to a slight change in the dynamical system's state, there is a slight change in these numbers, which creates or modifies the geometric shapes of the system's states in space [3].

In systems science, a static system means that the system's form and parameters do not change over time [2]. Nevertheless, a dynamical system whose behavior undergoes severe oscillations and fluctuations due to a tiny change in its parameters is more interesting. For example, the weather and climate of a geographical area have this typical behavior, for which a minor fluctuation in a variable, even in the fourth to sixth decimal places, can completely change the result of the weather forecast [4]. Linear systems, however, do not have this behavior, and the system's trajectories depend entirely on their initial states [5]. Today, the modeling of complex dynamical systems is developed and applied in many fields, such as meteorology [4,6], geology [7], mass and heat transfer [8], oceanography, fluid mechanics [1], and gravity and cosmology [9].

Nonlinear dynamical systems are essential frameworks for chaos theory [10,11]. In a general dynamical system, an attractor is defined as a set of numerical values that the system's trajectory evolves towards for a wide range of initial values [12]. If the system is structurally stable, when the numerical values of the system's trajectory are sufficiently close to the attractor, even if there is a slight disturbance, the system's trajectory remains close to the attractor [13]. In other words, an attractor is the limit set of the system's solutions as time evolves long enough, mathematically

To cite this article:
T. Moalemi, A. Ahmadi, S. Jafari, G. Chen "A novel mega-stable system with attractors in real-life object shapes", *Scientia Iranica* (2025) **32**(10): 7030.
https://doi.org/10.24200/sci.2023.60858.7030

approaching infinity [14]. An attractor is a region in the system's state space, usually having physical [15] or economical [16,17] meanings, etc.

More interestingly, a dynamical system can have coexisting attractors, which can be obtained from a single system with different initial conditions [18,19]. A multi-stable system is a system that can produce coexisting attractors [20,21]. Multi-stable systems can be roughly classified into mega-stable [22,23] and extreme multi-stable [24,25] systems. If the number of coexisting attractors is small, the system is referred to as a mega-stable system [26,27], while if the coexisting attractors are numerous, the system is classified as an extreme multi-stable system [28,29]. These systems have vibrant dynamics compared to mono-stable ones, attracting increasing attention recently [30-32].

Tang et al. in 2018 [22] introduced a novel mega-stable nonlinear system called the carpet oscillator. This name was given to this system because of the patterns of its coexisting hidden and self-excited attractors, which looked like a Persian carpet. Vo et al. in 2019 [23] gained a giga-stable system by forcing a mega-stable system with its twin. In the same year, Tuna et al. reported a mega-stable hyper-jerk system with multi-wing attractors [33]. In 2020, Akgul et al. [26] achieved mega-stability in a chaotic system without applying the forcing term. In the same year, Chen et al. [27] detected mega-stability in dynamical systems with various attractors, including torus, chaotic and hyperchaotic attractors. Karami et al., in 2021 [34], investigated a new mega-stable system with attractors that have irregular patterns; also, spatially square wave damping was applied to this system. Karami et al. [35] reached a new mega-stable system with triangular wave damping a year later. In 2022 Li et al. [36] applied a memristor to a mega-stable system without the forcing term, and its mega-stability depended on its Hamiltonian energy. Vijayakumar et al. [37] examined a similar system with repelling, conservative and dissipative dynamics in the same year.

In this paper, a two-dimensional autonomous nonlinear dynamical system is proposed, which has very rich dynamical behaviors in the sense that it not only can generate multiple coexisting attractors and thus is mega-stable but also can change the shapes of the attractors via parameter variations. The remainder of the paper is organized as follows. Section 2 introduces the new system. Main simulation results with different initial conditions are presented to show the coexisting attractors and the variety of the patterns of the coexisting attractors that resemble the shapes of some real-life objects. Afterward, the equilibrium points of the introduced system are calculated, and their stability is reported in Section 3. Furthermore, the energy dissipation of this system is analyzed, and its analog circuit is implemented in Section 4. Section 5 discusses some basic properties of the new system and summarizes the paper.

2. The proposed mega-stable system and results

The proposed mega-stable dynamical system is described by System (1):

$$\begin{cases} \dot{x} = \tanh(y) + a\cos(by) \\ \dot{y} = -\tanh(x) + \tanh(10y)\cos(x) \end{cases} \quad (1)$$

This system is a simple two-dimensional nonlinear autonomous system with some trigonometric functions, where a and b are real parameters that can be used to change the shape of the coexisting attractors, as further demonstrated below.

The dynamical behaviors of System (1) are incredibly complex; therefore, they are investigated with numerical simulations. In Figures 2-5, part (a) depicts the result of simulating the system with an arbitrary set of initial conditions shown by red dots. The runtime for simulations is set to 5000. The transient parts of the trajectories, the first 90% of the total runtime, are plotted in cyan. The last 10% of the trajectories, considered steady-state segments, are plotted in navy blue. Part (b) displays the coexisting attractors; meanwhile, the initial conditions and the transient phases are not shown. The attractors of this system are all limit cycles that, although they vary in size, are almost the same in shape and form for a particular set of parameters. Part (c) demonstrates each attractor and its corresponding basin of attraction in different colors. Part (d) illustrates the corresponding real-life objects with similar shapes as the coexisting attractors, which shows an interesting good match.

In the first case, consider $a = 1, b = 0.5$, and simulate the system with these parameters. The results are shown in Figure 1. In Figure 1(a), the trajectories correspond to 21 different initial conditions, distributed along the x-axis from $x = -50$ to $x = 50$ with a step size of 5. A small random number between zero and one, acting as a perturbation, disturbs their positions on the y-axis. Briefly, the system's attractors look like a Persian decorative rug.

Now, assume that parameter a is the same as before, but parameter b is reduced to 0.01. The numerical results of System (1) with this set of parameters are shown in Figure 2. The interval of the initial conditions is the same as before. However, to better detect the coexisting attractors, the step size is lowered by one and now is 4. Thus, 26 different initial conditions are used for obtaining the results shown in Figure 2. Amazingly, the pattern of coexisting attractors is changed from a Persian rug to a kind of nut, i.e., chestnut, by just changing one of the system's parameters.

Again, parameter a is kept constant, but parameter b is multiplied by 10, i.e., it is equal to 0.1 now. The initial conditions are like the case of Figure 2. New results produced by this parameter variation are shown in Figure 3. Although the lower part of the coexisting attractors has almost the same form as before, the upper part is changed prominently. As a result, the pattern of the attractors is entirely different from the chestnut, but it is transformed into pears. Interestingly, a nut shape is changed to a kind of fruit shape.

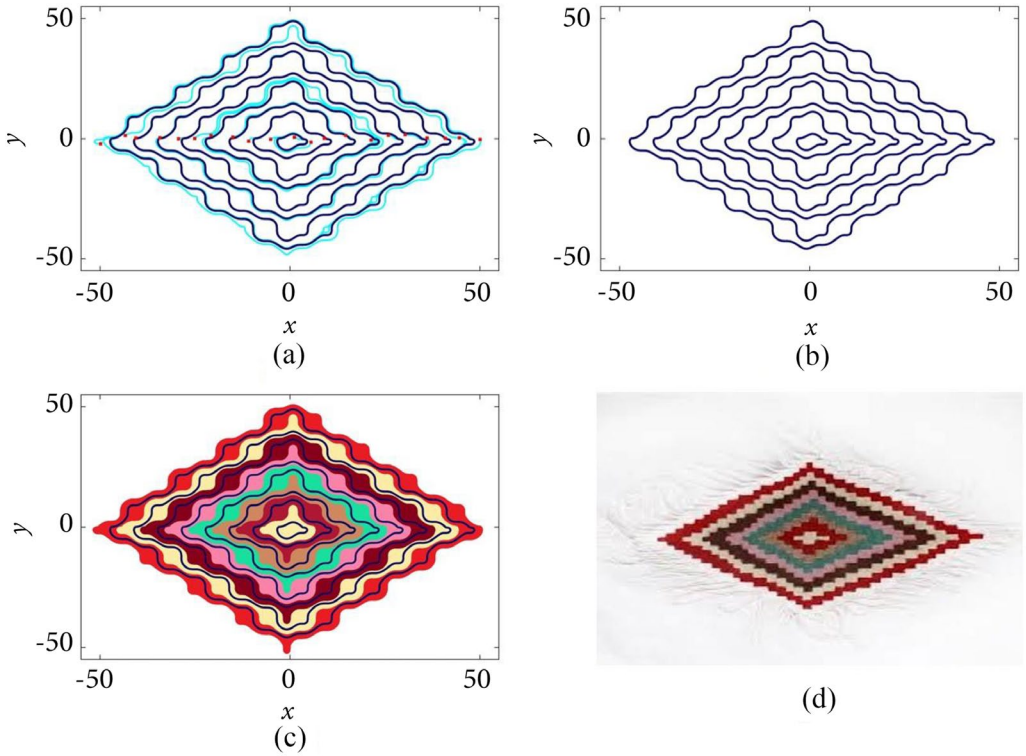

Figure 1. (a) Trajectories of System (1), with $a = 1, b = 0.5$, for 21 different initial conditions located on a line ($x = -50$ to $x = 50$ with step-size 5. Random values around zero are considered for y), which are shown by red dots. The runtime is set to 5000 for all trajectories. The transient parts of trajectories are shown by cyan dots, which cover 90% of the total runtime. The steady-state part of each trajectory, over the last 10% of runtime, is shown in navy blue. (b) Only the steady-state part of the trajectories is shown. (c) Basin of attraction. (d) A Persian decorative rug.

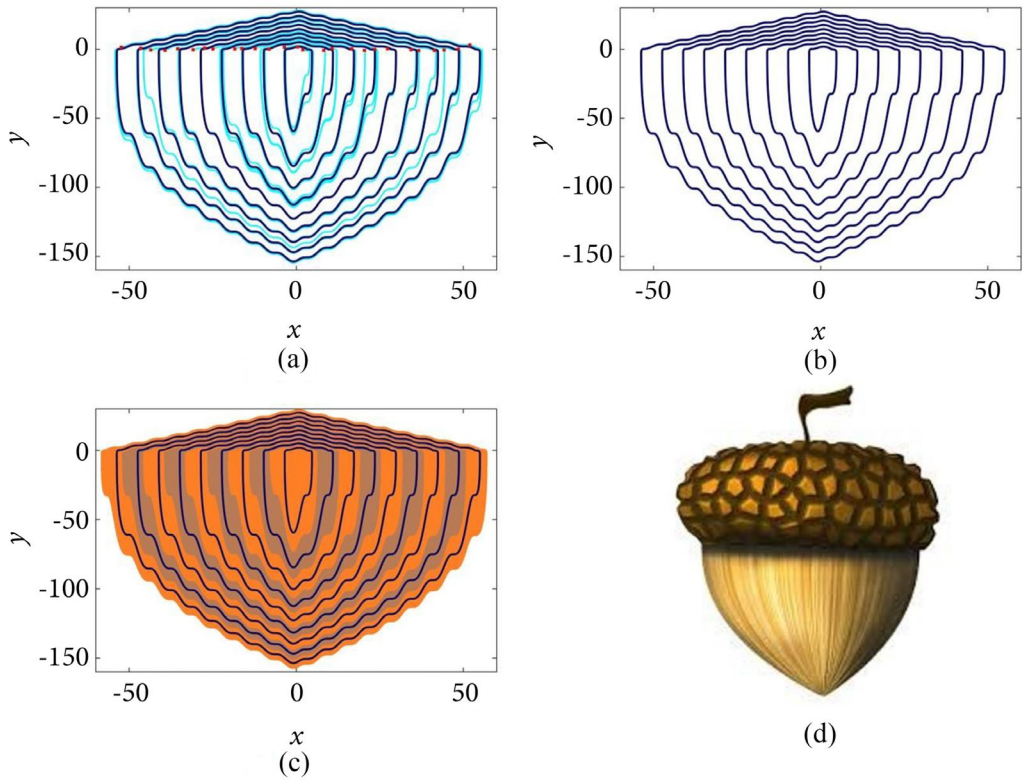

Figure 2. (a) Trajectories of System (1) with $a = 1, b = 0.01$, for 26 different initial conditions located on a line ($x = -50$ to $x = 50$ with step-size 4. Random values around zero are considered for y), which are shown by red dots. The runtime is set to 5000 for all trajectories. The transient parts of trajectories are shown by cyan dots, which cover 90% of the total runtime. The steady-state part of each trajectory, over the last 10% of runtime, is shown in navy blue. (b) Only the steady-state part of the trajectories is shown. (c) Basin of attraction. (d) A chestnut.

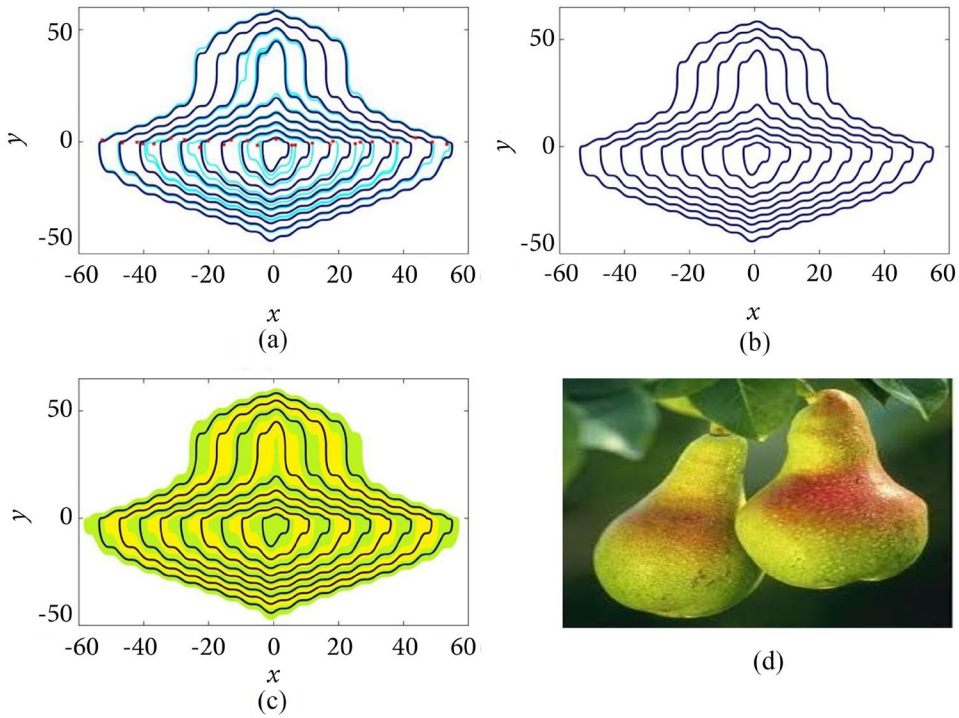

Figure 3. (a) Trajectories of System (1) with $a = 1, b = 0.1$, for 26 different initial conditions located on a line ($x = -50$ to $x = 50$ with step-size 4. Random values around zero are considered for y), which are shown by red dots. The runtime is set to 5000 for all trajectories. The transient parts of trajectories are shown by cyan dots, which cover 90% of the total runtime. The steady-state part of each trajectory, over the last 10% of runtime, is shown in navy blue. (b) Only the steady-state part of the trajectories is shown. (c) Basin of attraction. (d) Two pears.

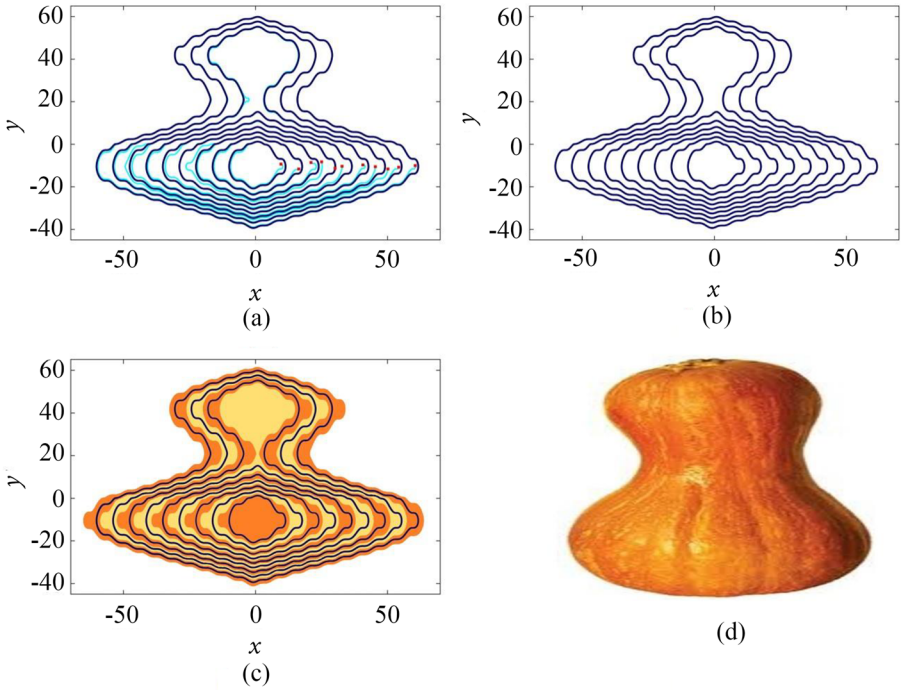

Figure 4. (a) Trajectories of System (1) with $a = 2, b = 0.1$, for 11 different initial conditions located on a line (x=10 to x=60 with step-size 5. Random values around -10 are considered for y), which are shown by red dots. The runtime is set to 5000 for all trajectories. The transient parts of trajectories are shown by cyan dots, which cover 90% of the total runtime. The steady-state part of each trajectory, over the last 10% of runtime, is shown in navy blue. (b) Only the steady-state part of the trajectories is shown. (c) Basin of attraction. (d) A pumpkin.

After investigating the effect of parameter b on the patterns of the coexisting attractors, parameter a is varied next. In all previous simulations, parameter a was fixed at 1. In Figure 4, the variation of the attractors' shapes is studied by duplicating parameter a. Totally 11 different initial conditions, from $x = 10$ to $x = 60$ with a step size of 5, are utilized to perform the simulations. From now on, the initial conditions are not along the $y = 0$ line anymore; they are along the $y = -10$ line, subject to some slight disturbance. By setting $a = 2, b = 0.1$, where the parameter b is now kept unchanged, the attractors

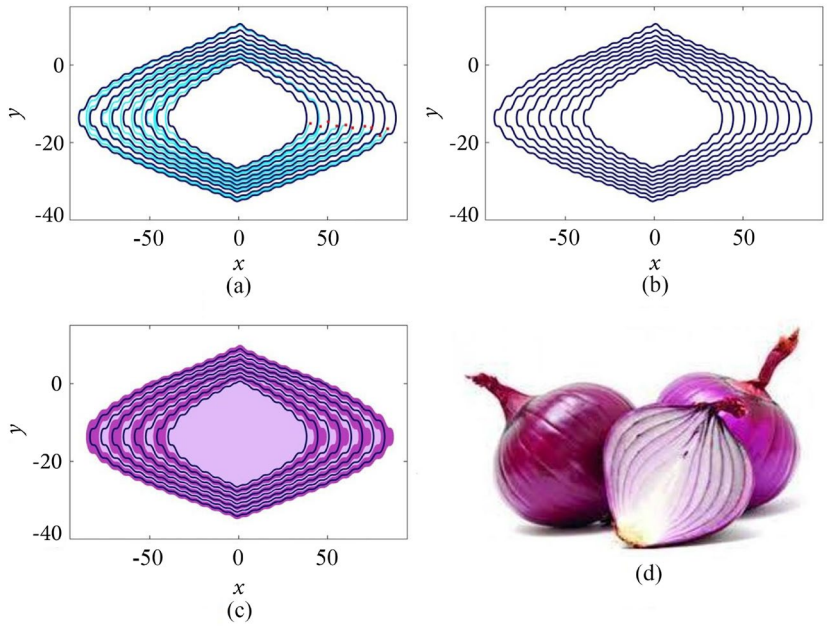

Figure 5. (a) Trajectories of System (1) with a=5, b=0.1, for 10 different initial conditions located on a line (x=40 to x=85 with step-size 5. Random values around -15 are considered for y), which are shown by red dots. The runtime is set to 5000 for all trajectories. The transient parts of trajectories are shown by cyan dots, which cover 90% of the total runtime. The steady-state part of each trajectory, over the last 10% of runtime, is shown in navy blue. (b) Only the steady-state part of the trajectories is shown. (c) Basin of attraction. (d) Onions.

tend to form two distinct parts connected with a bottleneck. This appearance resembles the shape of a pumpkin, a type of vegetable.

To show one more pattern, parameter b is kept constant, but parameter a is increased to 5. The numerical result of using ten different initial conditions from $x = 40$ to $x = 85$ with a step size of 5 is depicted in Figure 5. The initial conditions are located around the $y = -15$ line. With this parameter change, the upper part of the attractors in Figure 4 diminished, but a uniform shape was formed. In this case, the layered structure of the coexisting attractors is analogous to the onions.

3. Fixed points stability and dissipation study

Equilibrium points of a dynamical system are points in which the velocity of all state variables becomes zero. These points can be obtained by setting the right-hand side of the system's differential equations to zero. The y values of the equilibrium points of System (1) are obtained by solving the $\dot{x} = 0$ equation and then by substituting these values in the $\dot{y} = 0$ equation, the corresponding x values are achieved. System (1) cannot be solved analytically, but some realistic assumptions can ease the problem. Since System (1) includes $\tanh$ functions and this trigonometric function rapidly converges to 1 for positive inputs and -1 for negative inputs, all $\tanh$ functions are substituted by ± 1, and the equations are solved. This procedure for different values of parameter a (1, 2, and 5) is shown in Eqs. (2), (3), and (4), respectively. Since the $\tanh$ functions converge to different values for positive and negative inputs, each parameter leads to various sets of solutions that shown in Box I.

The above answers are valid only after the convergence of the $\tanh$ functions. For values of x, y in which the $\tanh$ functions have not been converged yet, a numerical method is employed. This technique is based on the fact that in equilibrium points, the value of $Z = \dot{x}^2 + \dot{y}^2$ is equal to zero. Moreover, the Poincaré-Bendixon theory says that "every cycle or limit cycle in two dimensions must surround at least one equilibrium point". Hence by varying the values of x, y in the interval corresponding to the region of the innermost limit cycles with a fixed step size of 0.01, the value of Z is calculated. Afterward, based on the least values of this function, a threshold is applied to the values, and those points with lower Z values are considered equilibrium points. Since all limit cycles surround these equilibrium points, the Poincaré-Bendixon theory is satisfied. The results of numerical simulations for different pairs of parameters are depicted in Figures 6-10. Part (a) of all these figures illustrates the Z surface, and part (b) demonstrates the obtained equilibrium points by magenta color. For $a = 1, b = 0.5$, x and y are varied in $[-3.34, 4.53]$ and $[-4.8, 2.01]$, respectively. By setting the threshold as 10^{-5}, ten equilibrium points are obtained and shown in Figure 6(b).

The results for $a = 1, b = 0.01$, varying x in $[-3.42, 4.7]$ and y in $[-60, 2]$ are shown in Figure 7. After applying a threshold of 10^{-7}, 45 points are obtained. If the value of a is kept fixed, but the value of b is multiplied by 10, the outcomes are like Figure 8. In this figure, x is varied in $[-3.4, 4.7]$, and y is varied in $[-13.1, 1.85]$. In this case, just one point is achieved considering a threshold like the former.

$$(x,y):\left\{y=\left\{\begin{array}{ll}\dfrac{(2k+1)\pi}{b} & k\in\mathbb{W},y>0\rightarrow x=\left\{\begin{array}{ll}(2k)\pi & k\in\mathbb{N},x>0\\ -(2k+1)\pi & k\in\mathbb{W},x<0\end{array}\right.\\ \dfrac{-(2k)\pi}{b} & k\in\mathbb{N},y<0\rightarrow x=\left\{\begin{array}{ll}(2k+1)\pi & k\in\mathbb{W},x>0\\ -(2k)\pi & k\in\mathbb{N},x<0\end{array}\right.\end{array}\right.\right\} \tag{2}$$

$$(x,y):\left\{y=\left\{\begin{array}{ll}\dfrac{1}{b}\left(\dfrac{2\pi}{3}\right),\dfrac{1}{b}\left(\pm\dfrac{2\pi}{3}+2k\pi\right) & k\in\mathbb{N},y>0\rightarrow x=\left\{\begin{array}{ll}(2k)\pi & k\in\mathbb{N},x>0\\ -(2k+1)\pi & k\in\mathbb{W},x<0\end{array}\right.\\ -\dfrac{1}{b}\left(\dfrac{\pi}{3}\right),-\dfrac{1}{b}\left(\pm\dfrac{\pi}{3}+2k\pi\right) & k\in\mathbb{N},y<0\rightarrow x=\left\{\begin{array}{ll}(2k+1)\pi & k\in\mathbb{W},x>0\\ -(2k)\pi & k\in\mathbb{N},x<0\end{array}\right.\end{array}\right.\right\} \tag{3}$$

$$(x,y):\left\{y=\left\{\begin{array}{ll}\dfrac{1}{b}(1.7722),\dfrac{1}{b}(\pm1.7722+2k\pi) & k\in\mathbb{N},y>0\rightarrow x=\left\{\begin{array}{ll}(2k)\pi & k\in\mathbb{N},x>0\\ -(2k+1)\pi & k\in\mathbb{W},x<0\end{array}\right.\\ -\dfrac{1}{b}(1.3694),-\dfrac{1}{b}(\pm1.3694+2k\pi) & k\in\mathbb{N},y<0\rightarrow x=\left\{\begin{array}{ll}(2k+1)\pi & k\in\mathbb{W},x>0\\ -(2k)\pi & k\in\mathbb{N},x<0\end{array}\right.\end{array}\right.\right\} \tag{4}$$

Box I.

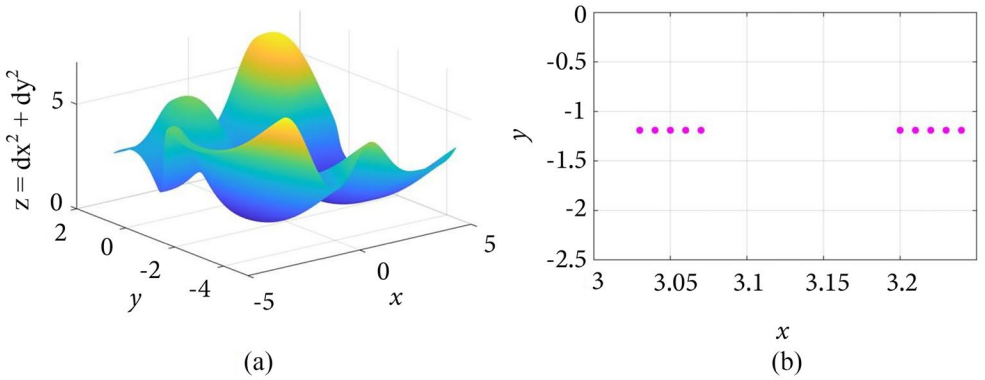

Figure 6. (a) $Z=\dot{x}^2+\dot{y}^2$ surface of System (1) with $a=1, b=0.5$, while x is in the interval $x=-3.34$to $x=4.53$ and y is in the interval y=−4.8 to y=2.01 with steps equal to 0.01. (b) The points of the Z surface whose distance from the Z=0 plane is less than the threshold of 10^{-5} are shown by magenta dots (10 points).

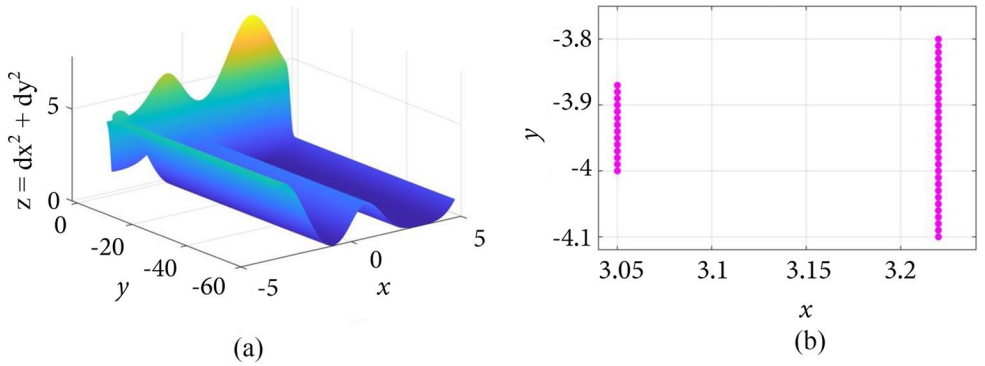

Figure 7. (a) $Z=\dot{x}^2+\dot{y}^2$ surface of System (1) with $a=1, b=0.01$, while x is in the interval $x=-3.42$ to $x=4.7$ and y is in the interval $y=-60$ to $y=2$ with steps equal to 0.01. (b) The points of the Z surface whose distance from the $Z=0$ plane is less than the threshold of 10^{-7} are shown by magenta dots (45 points).

In Figures 9 and 10, the value of b has not been changed, but the value of a is multiplied by 2 and 5, respectively. x values of Figure 9 are varied in $[-10, 11.36]$, and y values are varied in $[-20.8, 1.24]$. Applying the threshold at 10^{-6}, results in 22 final points. In Figure 10, the variation of x is limited in the interval $[-39.71, 38.26]$, and y is limited in the interval $[-26.56, 0.61]$. In this case, 292 points are obtained after applying a 10^{-5} threshold.

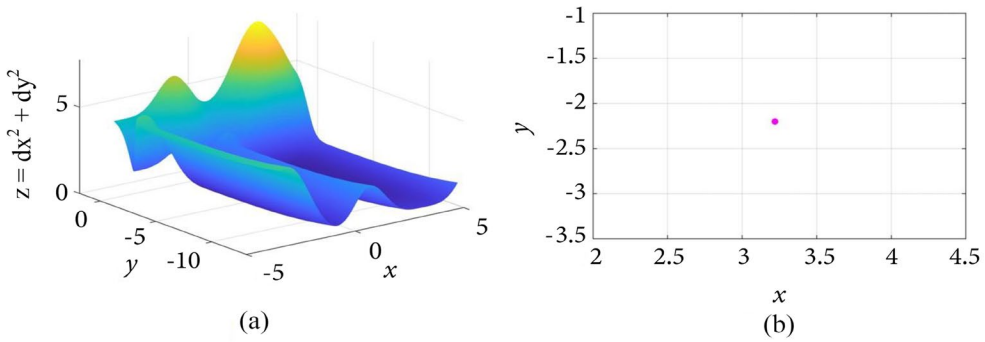

Figure 8. (a) $Z = \dot{x}^2 + \dot{y}^2$ surface of System (1) with $a = 1, b = 0.1$, while x is in the interval $x = -3.4$ to $x = 4.7$ and y is in the interval $y = -13.1$ to $y = 1.85$ with steps equal to 0.01. (b) The points of the Z surface whose distance from the $Z = 0$ plane is less than the threshold of 10^{-7} are shown by magenta dots (one point).

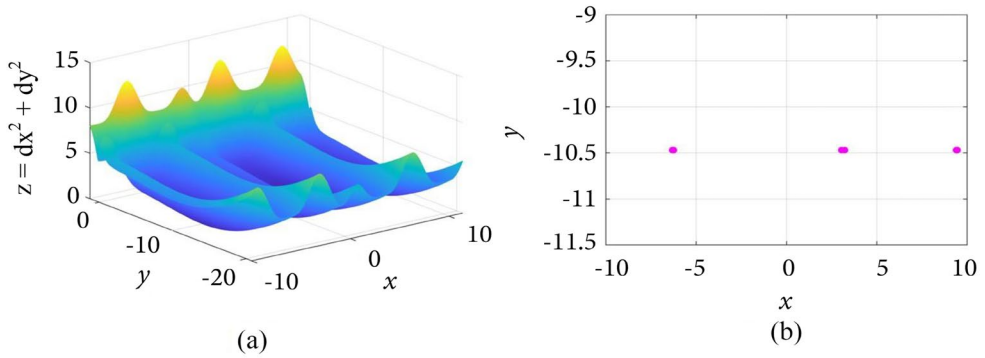

Figure 9. (a) $Z = \dot{x}^2 + \dot{y}^2$ surface of System (1) with $a = 2$, $b = 0.1$, while x is in the interval x =−10 to x = 11.36 and y is in the interval $y = -20.8$ to $y = 1.24$ with steps equal to 0.01. (b) The points of the Z surface whose distance from the $Z = 0$ plane is less than the threshold of 10^{-6} are shown by magenta dots (22 points).

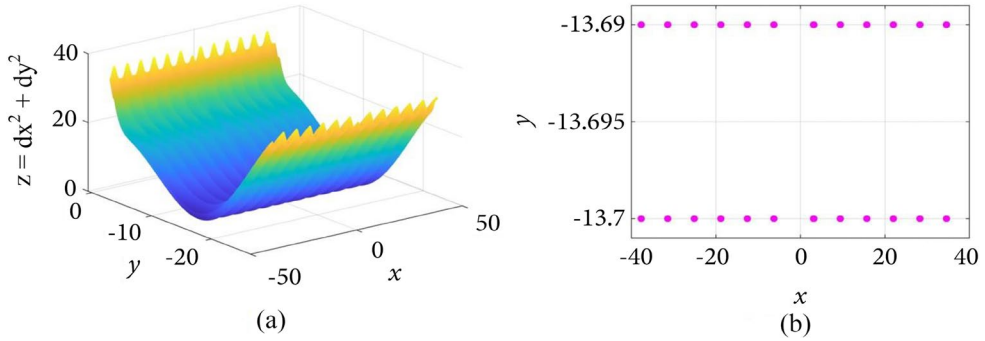

Figure 10. (a) $Z = \dot{x}^2 + \dot{y}^2$ surface of System (1) with $a = 5, b = 0.1$, while x is in the interval $x = -39.71$to $x = 38.26$ and y is in the interval $y = -26.56$ to $y = 0.61$ with steps equal to 0.01. (b) The points of the Z surface whose distance from the $Z = 0$ plane is less than the threshold of 10^{-5} are shown by magenta dots (292 points).

To study the stability of the equilibrium points, the Jacobian matrix of the dynamical system should be obtained, and it must be linearized around the equilibrium points. The real parts of the linearized Jacobian matrix's Eigenvalues indicate the equilibrium point's stability. The equilibrium point is stable only if all the Eigenvalues have negative real parts. The appearance of an Eigenvalue with a positive real part lead to unstability. There can be Eigenvalues with zero real parts; in these cases, the stability analysis cannot be conducted based on the Eigenvalues and requires more study. The Jacobian matrix of System (1) can be written as Eq. (5).

In the last part of this equation, the values of tanh functions are replaced with ± 1, and their derivatives are replaced with zero. In Eq. (6), the characteristic equation of this matrix is obtained by setting the $|\lambda \boldsymbol{I}_n - \boldsymbol{J}|$ equal to zero. This characteristic equation has two zero roots that challenge the stability analysis of System (1)'s equilibrium points. Nevertheless, several random values of initial conditions were used in previous simulations, and none converged to an equilibrium point. Thus, all the equilibrium points of System (1) are unstable.

$$\boldsymbol{J} = \begin{bmatrix} 0 & \dfrac{1}{\left(\cosh(\mathrm{y})\right)^2} - ab\sin(\mathrm{by}) \\ -\dfrac{1}{\left(\cosh(\mathrm{x})\right)^2} - \sin(\mathrm{x})\tanh(10\mathrm{y}) & \dfrac{10\cos(x)}{\left(\cosh(10y)\right)^2} \end{bmatrix} \quad (5)$$

$$\rightarrow \boldsymbol{J} = \begin{bmatrix} 0 & -ab\sin(by) \\ \pm\sin(x) & 0 \end{bmatrix}$$

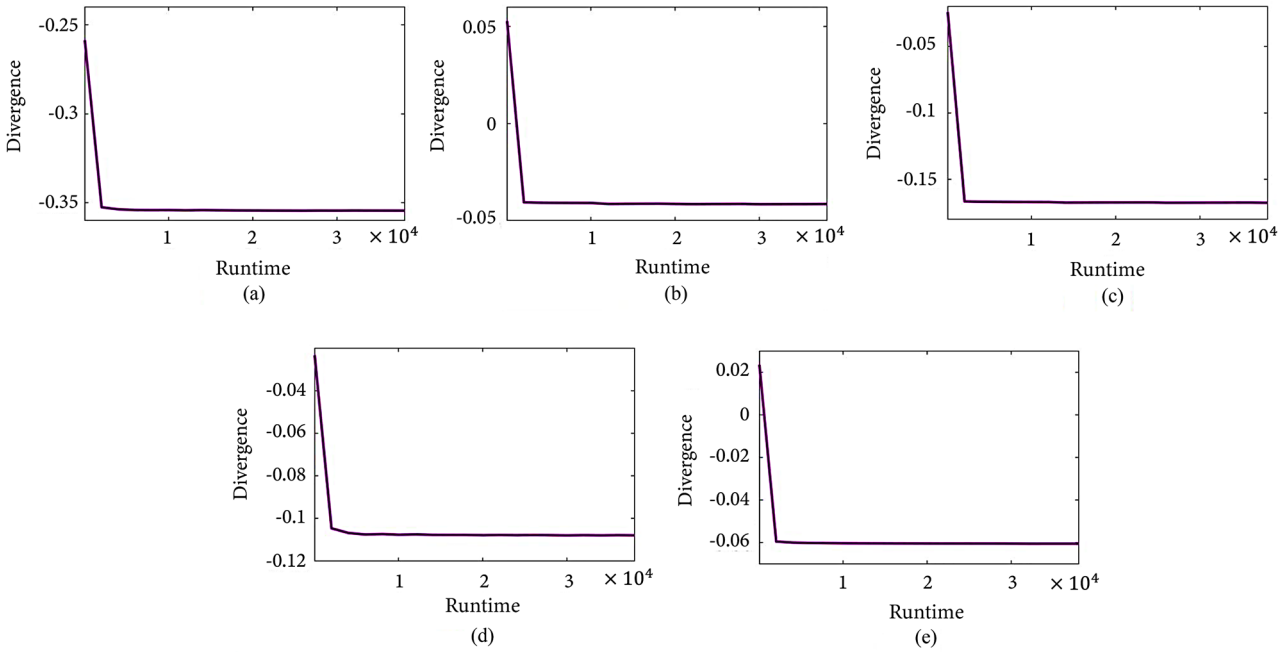

Figure 11. Divergence diagram of System (1) with initial conditions $(x_0, y_0) = (0, 0)$ and parameters (a) $a = 1, b = 0.5$, (b) $a = 1, b = 0.01$, (c) $a = 1, b = 0.1$, (d) $a = 2, b = 0.1$ and (e) $a = 5, b = 0.1$. The number to which the diagrams have converged indicates the energy consumption rate of the System (1) with these parameters. The energy consumption of System (1) for all pairs of parameters is a negative value, and thus it is a dissipative system.

$$\left|\lambda \boldsymbol{I}_n - \boldsymbol{J}\right| = 0 \rightarrow \begin{vmatrix} \lambda & \text{absin}(\text{by}) \\ \pm\sin(\text{x}) & \lambda \end{vmatrix} = \lambda^2 \pm ab\sin(by)\sin(x) = 0 \rightarrow \lambda^2 = 0 \rightarrow \lambda = 0. \quad (6)$$

The attraction ability of the cycles was observed in the previous numerical simulations like phase portraits and basins of attraction. This characteristic can be quantified by calculating the energy consumption of the dynamical system. This quantity is equal to the divergence of the system, i.e., the trace of the Jacobian matrix. This quantity can be positive, zero, or negative; the system is called explosive, conservative, and dissipative. If a system is dissipative, the trajectories in the state space are attractors. The divergence of System (1) is calculated as Eq. (7):

$$\nabla = Tr(\boldsymbol{J}) = 10\cos(x)\frac{1}{\left(\cosh(10y)\right)^2} = 10\cos(x)\left(\text{sech}(10y)\right)^2. \quad (7)$$

Since the divergence is state-dependent, its value cannot be obtained directly and requires numerical simulations. In Figure 11, System (1) is simulated with initial conditions located at the origin for runtime equal to 3.5×10^4 and the divergence is calculated with the help of average values of the $cos(x)\left(\text{sech}(10y)\right)^2$ term. Panels (a)-(e) portray the divergence of System (1) with different pairs of parameters. In all these diagrams, the value of the divergence converges to a negative quantity, which approves the dissipation of System (1). Furthermore, the cycles observed in previous numerical simulations are confirmed to be limit cycles.

4. Analog circuit design

In order to complete the performance study of System (1), it is necessary to conduct further experiments like designing its analog circuit. The analog circuit of System (1) is implemented in the simulation environment, and it is realized successfully. The designed circuit of System (1) for $a = 1$, $b = 0.5$ is shown in Figure 12 (x state variable) and Figure 13 (y state variable). The tanh functions are implemented using Q2N1711 bipolar transistors. Three tanh blocks are used in the circuit design, but as an example, just the first one in Figure 12 is discussed in detail. The mathematical formula governing the tanh block is written as Eq. (8). In this equation A is the gain that changes the amplitude of the resultant tanh and is modified by R_3, R_4, R_5, R_6, R_7 and the value of the current source I_1. The coefficient of the tanh block's input can be adjusted by R_1, R_2, and V_T. V_T is the thermal voltage of the transistors and $V_T \approx 26\,mV$ in room tempreture.

$$V_{out} = -A\tanh\left(\frac{R_2}{2R_1 V_T} V_{in}\right). \quad (8)$$

The supply voltages are $V_{CC} = 15$ V, $V_{EE} = -15$ V. For some pairs of parameters, the state variables' actual amplitude can lead to the circuit's saturation and malfunction; therefore, the circuit design is based on scaling all state variables to one-tenth of their actual value. The value of other components are $I_1 = I_2 = I_3 = 1.1$ mA,
$C_1 = C_2 = 10$ nF, $R_3 = R_4 = R_9 = R_{10} = R_{27} = R_{28} = 1$ kΩ,

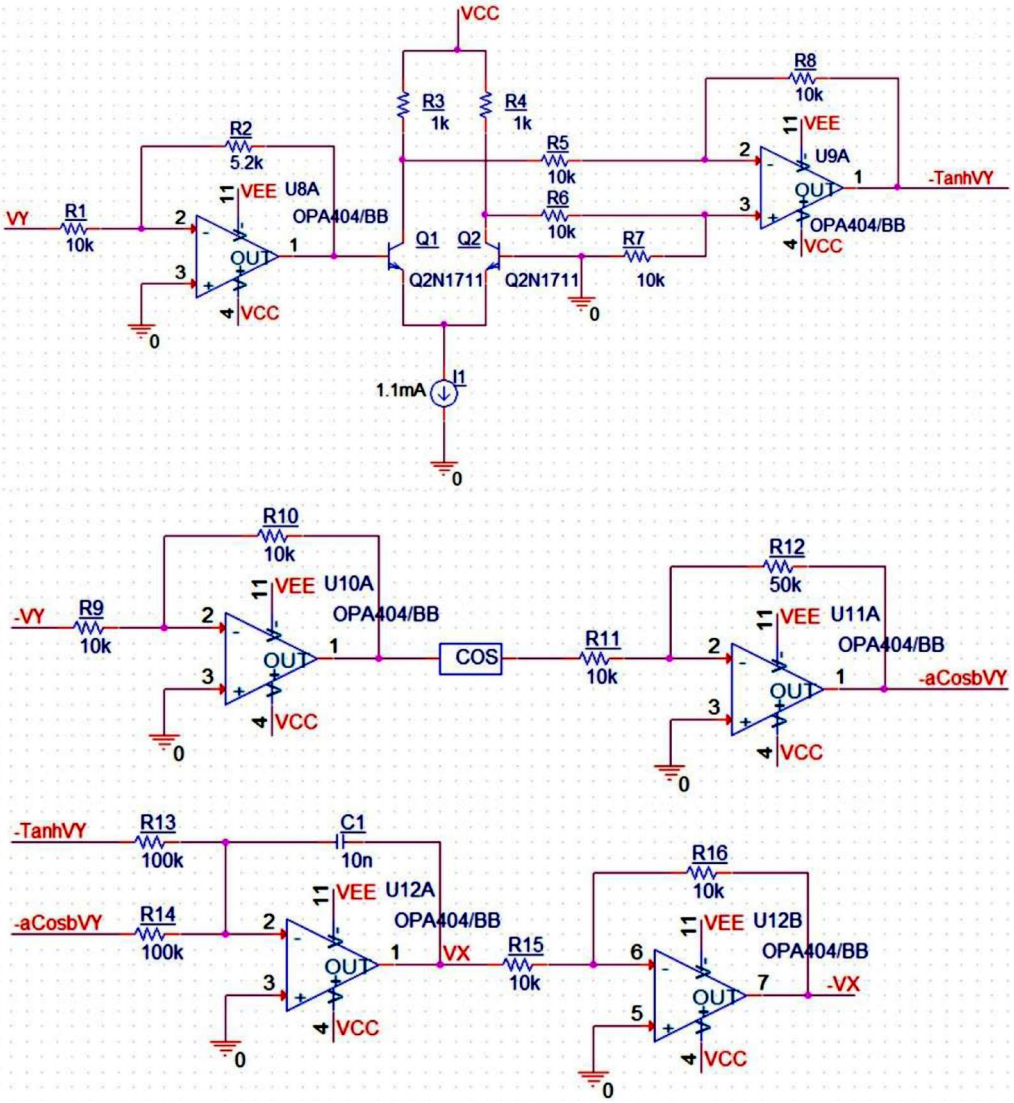

Figure 12. Analog circuit implementation of the *x* state variable of System (1) for $a = 1, b = 0.5$ and initial conditions $(x_0,\ y_0) = (0, 0)$.

$R_2 = R_{18} = 5.2\ \text{k}\Omega, R_1 = R_5 = R_6 = R_7 = R_9 = R_{11} = R_{15} = R_{16} = R_{17} = R_{21} = R_{22} = R_{23} = R_{24} = R_{25} = R_{29} = R_{30} = R_{31} = R_{32} = R_{33} = R_{37} = R_{38} = 10\ \text{k}\Omega$, $R_{26} = 52\ \text{k}\Omega, R_{13} = R_{14} = R_{35} = R_{36} = 100\ \text{k}\Omega$.

Parameter a is adjusted by varying R_{12} and parameter b is modified through R_{10}. For $a = 1, 2, 5$, the value of R_{12} is set to $10\ \text{k}\Omega, 20\ \text{k}\Omega, 50\ \text{k}\Omega$ and $R_{10} = 1\ \text{k}\Omega, 10\ \text{k}\Omega, 50\ \text{k}\Omega$ result in $b = 0.01, 0.1, 0.5$ respectively. The capacitors' initial conditions are all set to zero.

The designed circuit is simulated for previously used pairs of parameters, and the outcomes are depicted in Figure 14. Panels (a)-(e) correspond to $a = 1,\ b = 0.5,\ \ a = 1,\ b = 0.01, a = 1,\ b = 0.1, a = 2,\ b = 0.1,$ and $a = 5,\ b = 0.1,$ respectively. Comparing the circuit simulation results with previous numerical simulations proves the feasibility and availability of System (1). It should be noted that the attractors' shapes are like the innermost limit cycles obtained by numerical methods but differ in amplitude regarding the applied scaling.

5. Discussion and conclusion

A simple two-dimensional autonomous mega-stable dynamical system was proposed in this paper. The system inherits its nonlinearity from hyperbolic tangent and cosine functions. There are two parameters in the system, and careful numerical studies investigated their effects on the patterns of the coexisting attractors. The mega-stability and ability to produce different shapes of coexisting attractors were examined with fascinating findings: the patterns of the coexisting attractors resemble several real-life objects. Besides, the equilibrium points of the proposed system were obtained, and their stability was analyzed. They were all unstable fixed points. To approve the attraction of the observed coexisting cycles, the energy dissipation of this system was investigated, which led to a negative value. In other words, the system is dissipative, and all the cycles are limit cycles, not conservative ones. To confirm the availability of the limit cycles, an analog circuit simulation was conducted too, whose outcomes were consistent with

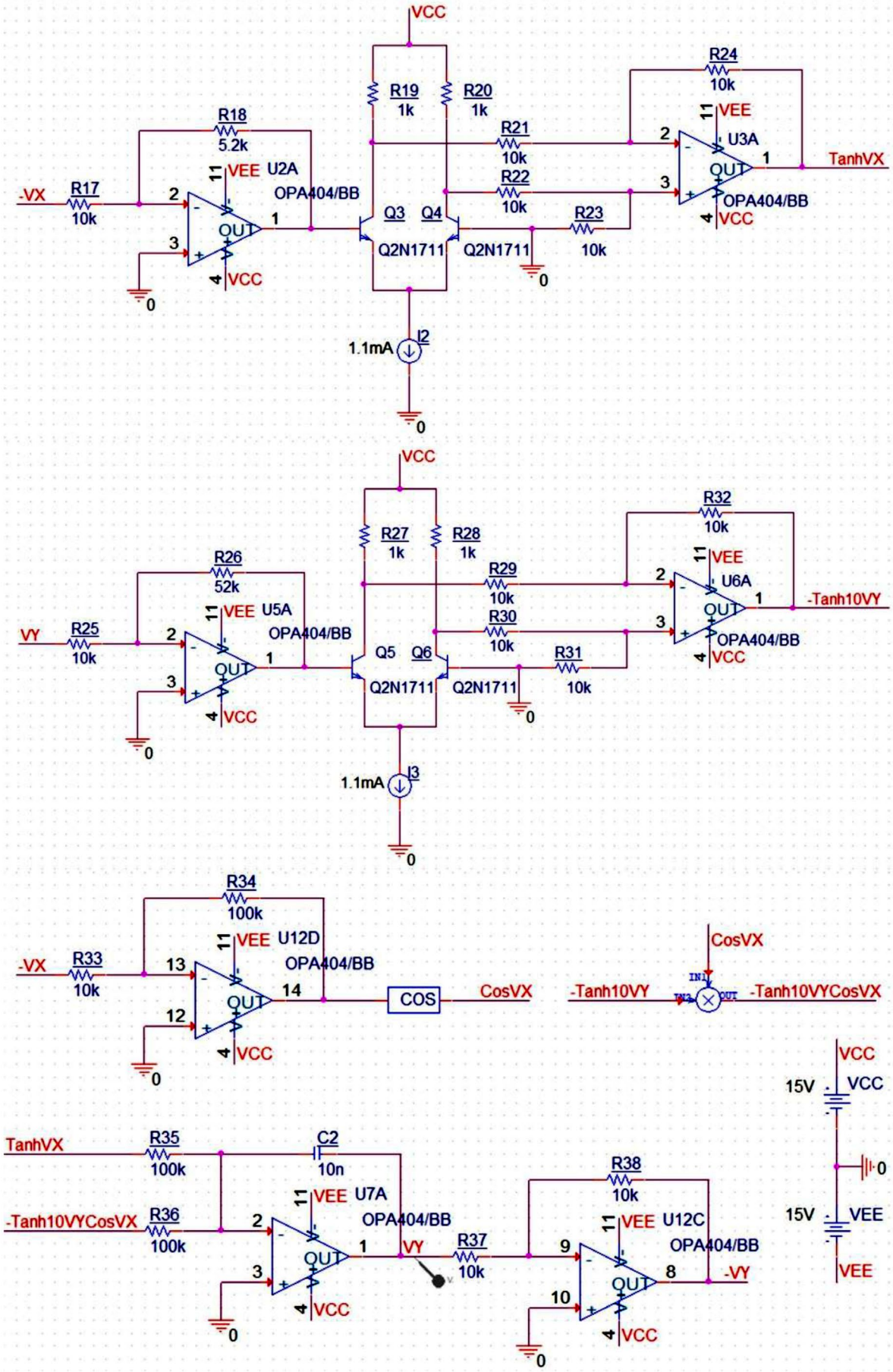

Figure 13. Analog circuit implementation of the y state variable of System (1) for $a = 1, b = 0.5$ and initial conditions $(x_0, y_0) = (0, 0)$.

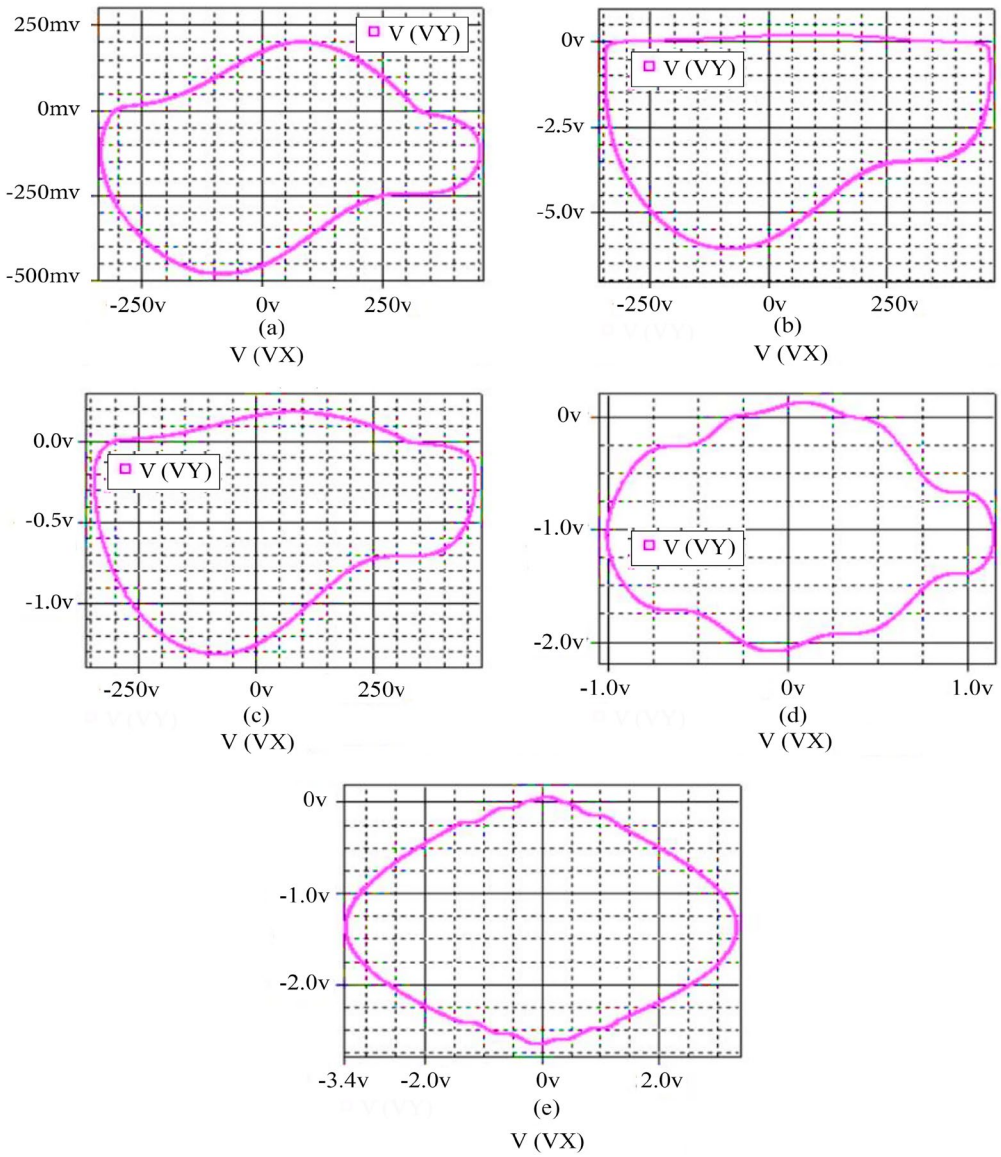

Figure 14. The simulation results of the analog circuit based on System (1). (a) $R_{10} = 50$ kΩ, $R_{12} = 10$ kΩ, (b) $R_{10} = 1$ kΩ, $R_{12} = 10$ kΩ, (c) $R_{10} = 10$ kΩ, $R_{12} = 10$ kΩ, (d) $R_{10} = 10$ kΩ, $R_{12} = 20$ kΩ, and (e) $R_{10} = 10$ kΩ, $R_{12} = 50$ kΩ. The initial conditions of all capacitors are zero. The shape of the results is consistent with the innermost limit cycles in numerical simulations, but their amplitude is one-tenth of the actual attractors.

previous numerical simulations. It is worth analyzing this newly introduced system's dynamical properties and unique features in the future with more complete and informative numerical diagrams and theoretical analysis. It is deemed that this highly flexible system would have a wide range of topological attractors to be revealed, and this unique system would have good potential for some new applications.

Funding

This research did not receive any specific grant from funding agencies in the public, commercial, or not-for profit sectors.

Conflicts of interest

The author is an Editorial Board Member for Scientia Iranica and was not involved in the editorial review or the decision to publish this article.

Authors contribution statement

First author: Methodology; Visualization; Writing – original draft

Second author: Formal analysis; Investigation; Writing – original draft

Third author: Conceptualization; Validation; Writing – review and editing

Fourth author: Project administration; Supervision; Writing – review and editing.

References

1. Tél, T., de Moura, A., Grebogi, C., et al. “Chemical and biological activity in open flows: A dynamical system approach”, *Physics Reports*, **413**(2-3), pp. 91-196 (2005). https://doi.org/10.1016/j.physrep.2005.01.005

2. Voss, H.U., Timmer, J., and Kurths, J. "Nonlinear dynamical system identification from uncertain and indirect measurements", *International Journal of Bifurcation and Chaos*, **14**(6), pp. 1905-1933 (2004). https://www.researchgate.net/publication/215554917

3. Kleeman, R. "Information theory and dynamical system predictability", *Entropy*, **13**(3), pp. 612-649 (2011). https://doi.org/10.3390/e13030612

4. Chernogor, L. and Rozumenko, V. "Earth–atmosphere–geospace as an open nonlinear dynamical system", *Radio Physics and Radio Astronomy*, **13**(2), p. 120 (2012).

5. Chen, Y., Georgiou, T.T., and Pavon, M. "Optimal transport over a linear dynamical system", IEEE *Transactions on Automatic Control*, **62**(5), pp. 2137-2152 (2016). https://doi.org/10.1109/TAC.2016.2602103

6. DeMaria, M. "A simplified dynamical system for tropical cyclone intensity prediction", *Monthly Weather Review*, **137**(1), pp. 68-82 (2009). https://doi.org/10.1175/2008MWR2513.1

7. Manzoni, S., Porporato, A., d'Odorico, P. et al. "Soil nutrient cycles as a nonlinear dynamical system", *Nonlinear Processes in Geophysics*, **11**(5/6), pp. 589-598 (2004). https://doi.org/10.5194/npg-11-589-2004

8. Dahlhaus, J., Edge, J., Tworzydło, J., et al. "Quantum Hall effect in a one-dimensional dynamical system", *Physical Review B*, **84**(11), 115133 (2011). https://doi.org/10.1103/PhysRevB.84.115133

9. Odintsov, S. and Oikonomou, V. "Autonomous dynamical system approach for *f(R)* gravity", *Physical Review D*, **96**, 104049 (2017). https://doi.org/10.1103/PhysRevD.96.104049

10. Kumar, S., Kumar, R., Cattani, C., et al. "Chaotic behavior of fractional predator-prey dynamical system", *Chaos, Solitons & Fractals*, **135**(1), 109811 (2020). https://doi.org/10.1016/j.chaos.2020.109811

11. Lin, H., Wang, C., Yu, F., et al. "An extremely simple multiwing chaotic system: Dynamics analysis, encryption application, and hardware implementation", IEEE *Transactions on Industrial Electronics*, **68**(12), pp. 12708-12719 (2021). https://doi.org/10.1109/TIE.2020.3047012

12. Deng, J., Zhou, M., Wang, C., et al. "Image segmentation encryption algorithm with chaotic sequence generation participated by cipher and multi-feedback loops", *Multimedia Tools and Applications*, **80**, pp. 13821-13840 (2021). https://doi.org/10.1007/s11042-020-10429-z

13. Leonov, G., Kuznetsov, N., and Vagaitsev, V. "Hidden attractor in smooth Chua systems", *Physica D: Nonlinear Phenomena*, **241**(18), pp. 1482-1486 (2012). https://doi.org/10.1016/j.physd.2012.05.016

14. Pehlivan, I., Moroz, I.M., and Vaidyanathan, S. "Analysis, synchronization and circuit design of a novel butterfly attractor", *Journal of Sound and Vibration*, **333**(20), pp. 5077-5096 (2014). https://doi.org/10.1016/j.jsv.2014.05.025

15. Munmuangsaen, B. and Srisuchinwong, B. "A new five-term simple chaotic attractor", *Physics Letters A*, **373**(44), pp. 4038-4043 (2009). https://doi.org/10.1016/j.physleta.2009.08.068

16. Kallosh, R., Linde, A., and Roest, D. "Universal attractor for inflation at strong coupling", *Physical Review Letters*, **112**, 011303 (2014). https://doi.org/10.1103/PhysRevLett.112.011303

17. Carrilho, P., Mulryne, D., Ronayne, J., et al. "Attractor behavior in multifield inflation", *Journal of Cosmology and Astroparticle Physics*, **2018**(06), 32 (2018). https://doi.org/10.1088/1475-7516/2018/06/032

18. Wang, Z., Moroz, I., Wei, Z., et al. "Dynamics at infinity and a Hopf bifurcation arising in a quadratic system with coexisting attractors", *Pramana*, **90**(1), article number 12 (2018). https://doi.org/10.1007/s12043-017-1505-x

19. Gong, L., Wu, R., and Zhou, N. "A new 4D chaotic system with coexisting hidden chaotic attractors", *International Journal of Bifurcation and Chaos*, **30**(10), 2050142 (2020). https://doi.org/10.1142/S0218127420501424

20. Lin, H., Wang, C., Hong, Q., et al. "A multi-stable memristor and its application in a neural network", *IEEE Transactions on Circuits and Systems II: Express Briefs*, **67**(12), pp. 3472-3476 (2020). https://doi.org/10.1109/TCSII.2020.3000492

21. Xu, Q., Cheng, S., Ju, Z., et al. "Asymmetric coexisting bifurcations and multi-stability in an asymmetric memristive diode-bridge-based jerk circuit", *Chinese Journal of Physics*, **70**, pp. 69-81 (2021). https://doi.org/10.1016/j.cjph.2020.11.007

22. Tang, Y., Abdolmohammadi, H.R., Khalaf, A.J.M., et al. "Carpet oscillator: A new megastable nonlinear oscillator with infinite islands of self-excited and hidden attractors", *Pramana*, **91**, article number 11 (2018). https://doi.org/10.1007/s12043-018-1581-6

23. Vo, T.P., Shaverdi, Y., Khalaf, A.J.M., et al. "A giga-stable oscillator with hidden and self-excited attractors: A megastable oscillator forced by his twin", *Entropy*, **21**(5), 535 (2019). https://doi.org/10.3390/e21050535

24. Bao, B.C., Xu, Q., Bao, H., et al. "Extreme multistability in a memristive circuit", Electronics Letters, **52**(12), pp. 1008-1010 (2016). https://doi.org/10.1049/el.2016.0563

25. Xu, Q., Liu, T., Feng, C.T., et al. "Continuous non-autonomous memristive Rulkov model with extreme multistability", *Chinese Physics B*, **30**(12), 128702 (2021). https://doi.org/10.1088/1674-1056/ac2f30

26. Akgul, A., Boyraz, O.F., Rajagopal, K., et al. "An unforced megastable chaotic oscillator and its application on protecting electrophysiological signals", *Zeitschrift für Naturforschung A*, **75**(12), pp. 1025-1037 (2020). https://doi.org/10.1515/zna-2020-0222

27. Chen, B., Rajagopal, K., Hamarash, I.I., et al. "Simple megastable oscillators with different types of attractors; tori, chaotic and hyperchaotic ones", *The European Physical Journal Special Topics*, **229**(6), pp. 1155-1161 (2020). https://doi.org/10.1140/epjst/e2020-900240-1

28. Chen, M., Sun, M., Bao, B., et al. "Controlling extreme multistability of memristor emulator-based dynamical circuit in flux–charge domain", *Nonlinear Dynamics*, **91**(2), pp. 1395-1412 (2018). https://doi.org/10.1007/s11071-017-3952-9

29. Chen, M., Sun, M., Bao, H., et al. "Flux–charge analysis of two-memristor-based Chua's circuit: Dimensionality decreasing model for detecting extreme multistability", IEEE *Transactions on Industrial Electronics*, **67**(3), pp. 2197-2206 (2019). https://doi.org/10.1109/TIE.2019.2907444

30. Rajagopal, K., Singh, J.P., Akgul, A., et al. "A novel dissipative and conservative megastable oscillator with engineering applications", *Modern Physics Letters B*, **34**(1), 2150007 (2020). https://doi.org/10.1142/S021798492150007X

31. Li, H., Bao, H., Zhu, L., et al. "Extreme multistability in simple area-preserving map", *IEEE Access*, **8**, pp. 175972-175980 (2020). https://doi.org/10.1109/ACCESS.2020.3026676

32. Gong, L.-H., Luo, H.-X., Wu, R.-Q., et al. "New 4D chaotic system with hidden attractors and self-excited attractors and its application in image encryption based on RNG", *Physica A: Statistical Mechanics and its Applications*, **591**, 126793 (2022). https://doi.org/10.1016/j.physa.2021.126793

33. Tuna, M., Karthikeyan, A., Rajagopal, K., et al. "Hyperjerk multiscroll oscillators with megastability: Analysis, FPGA implementation and a novel ANN-ring-based true random number generator", *AEU-International Journal of Electronics and Communications*, **112**, 152941 (2019). https://doi.org/10.1016/j.aeue.2019.152941

34. Karami, M., Ramamoorthy, R., Ali, A.M.A., et al. "Jagged-shape chaotic attractors of a megastable oscillator with spatially square-wave damping", *The European Physical Journal Special Topics*, **231**, pp. 2445-2454 (2022). https://doi.org/10.1140/epjs/s11734-021-00373-w

35. Karami, M., Ramakrishnan, B., Hamarash, I.I., et al. "Investigation of the simplest megastable chaotic oscillator with spatially triangular wave damping", *International Journal of Bifurcation and Chaos*, **32**(07), 2230016 (2022). https://doi.org/10.1142/S0218127422300166

36. Li, R., Dong, E., Tong, J., et al. "A new autonomous memristive megastable oscillator and its hamiltonian-energy-dependent megastability", *Chaos: An Interdisciplinary Journal of Nonlinear Science*, **32**(1), 013127 (2022). https://doi.org/10.1063/5.0066951

37. Vijayakumar, M., Natiq, H., Meli, M.I.T., et al. "Hamiltonian energy computation of a novel memristive mega-stable oscillator (MMO) with dissipative, conservative and repelled dynamics", *Chaos, Solitons & Fractals*, **155**(1), 111765 (2022). https://doi.org/10.1016/j.chaos.2021.111765

Biographies

Tayebe Moalemi was born in Malayer, Iran, in 2000. She graduated with a Mathematics and Physics Diploma, achieving a GPA of 19.98 in 2018. In 2022, she received her BSc degree in Biomedical Engineering from the Biomedical Engineering Department at Amirkabir University of Technology in Tehran, Iran, with a GPA of 19.56. Currently, she is studying for her M.S. in Biomedical Engineering (Bioelectric) at Amirkabir University of Technology. In addition, she has completed a course in Biological Signal Processing. Her research interests include nonlinear dynamics, networks and synchronization, chaos theory, and their application in biomedical engineering.

Atefeh Ahmadi was born in Tehran, Iran, in 1996. She obtained a BSc and an MSc in Biomedical Engineering from Amirkabir University of Technology (Tehran Polytechnic) in 2018 and 2021, respectively. She is currently a PhD student at Amirkabir University of Technology, working under the guidance of Dr. Sajad Jafari (Tehran Polytechnic). She is interested in chaos theory, nonlinear dynamics, dynamical systems, and mathematical modeling.

Sajad Jafari was born in Kermanshah, Iran, in 1983. He received his BSc, MSc, and PhD in Biomedical Engineering in 2005, 2008, and 2013 from the Biomedical Engineering Department, Amirkabir University of Technology (Tehran Polytechnic), Tehran, Iran. He is currently an Assistant Professor there (since 2013). His research interests include nonlinear and chaotic systems and signals and mathematical biology. He is also interested in complex networks and collective behaviors, such as synchronization, Chimera states, and spiral waves. He serves as Editor in the

International Journal of Bifurcation and Chaos, the International Journal of Electronics and Communications, and Radio Engineering. He has been one of the highly cited Researchers in 2019 and 2020, according to Clarivate Analytics. He also has won the COMSTECH award in mathematics (2019).

Guanrong (Ron) Chen received an MSc in Computational Mathematics from Sun Yat-sen (Zhongshan) University, China, in 1981 and a PhD in applied Mathematics from Texas A&M University, USA, in 1987. He has been a Chair Professor (now, "Shun Hing Education and Charity Fund Chair Professorship in Engineering") and the Founding Director of the *Centre for Complexity and Complex Networks* at the City University of Hong Kong since the year 2000; prior to that, he was a tenured full Professor at the University of Houston, Texas, USA. He was elected a Member of the Academy of Europe (Academia Europaea) in 2014 and a Fellow of The World Academy of Sciences in 2015. In the past, he was elected IEEE Fellow in 1997 and became Life Fellow in 2019. He was conferred Honorary Doctorates by Saint Petersburg State University, Russia, in 2011 and by the University of Le Havre, Normandy, France, in 2014. He is a Highly Cited Researcher in Engineering and Mathematics according to Thomson Reuters (now Clarivate Web of Science), was the 2011 Euler Gold Medalist named by the Euler Foundation of Russia, and was the recipient of 2008, 2012, and 2016 Chinese State Natural Science Awards as well as eight best journal paper awards. He is Honorary Professor at different ranks in some 30 universities worldwide. Professor Chen's primary research pursuit is in nonlinear systems control and dynamics, as well as complex networks. He is the Editor-in-Chief of the International Journal of Bifurcation and Chaos.